



HAL
open science

Internal Energy Distribution of Secondary Ions Under Argon and Bismuth Cluster Bombardments: “Soft” Versus “Hard” Desorption–Ionization Process

Tingting Fu, Serge Della-Negra, David Touboul, Alain Brunelle

► **To cite this version:**

Tingting Fu, Serge Della-Negra, David Touboul, Alain Brunelle. Internal Energy Distribution of Secondary Ions Under Argon and Bismuth Cluster Bombardments: “Soft” Versus “Hard” Desorption–Ionization Process. *J.Am.Soc.Mass.Spectrom.*, 2018, 30 (2), pp.321-328. 10.1007/s13361-018-2090-z . hal-02024237

HAL Id: hal-02024237


<https://hal.science/hal-02024237>

Submitted on 21 Aug 2020

HAL is a multi-disciplinary open access archive for the deposit and dissemination of scientific research documents, whether they are published or not. The documents may come from teaching and research institutions in France or abroad, or from public or private research centers.

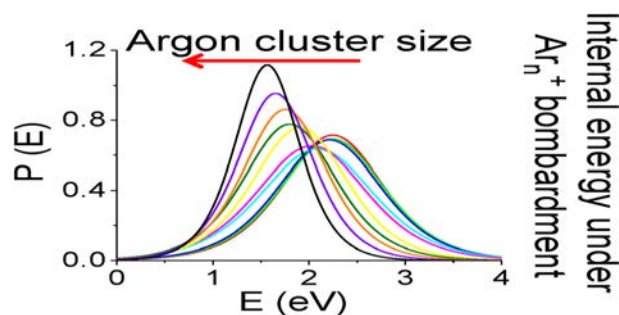
L'archive ouverte pluridisciplinaire **HAL**, est destinée au dépôt et à la diffusion de documents scientifiques de niveau recherche, publiés ou non, émanant des établissements d'enseignement et de recherche français ou étrangers, des laboratoires publics ou privés.

Internal Energy Distribution of Secondary Ions Under Argon and Bismuth Cluster Bombardments: “Soft” Versus “Hard” Desorption–Ionization Process

Tingting Fu,^{1,2} Serge Della-Negra,² David Touboul,¹  Alain Brunelle¹

¹Institut de Chimie des Substances Naturelles, CNRS UPR 2301, Université Paris-Sud, Université Paris-Saclay, Avenue de la Terrasse, 91198, Gif-sur-Yvette, France

²Institut de Physique Nucléaire, UMR 8608, IN2P3-CNRS, Université University Paris-Sud, Université Paris-Saclay, 15 rue Georges Clémenceau, 91406, Orsay, France



Abstract. The emission/ionization process under massive argon cluster bombardment was investigated by measuring the internal energy distributions of a series of benzylpyridinium ions. Argon clusters with kinetic energies between 10 and 20 keV and cluster sizes ranging from 500 to 10,000 were used to establish the influence of their size, energy, and velocity on the internal energy distribution of the secondary ions. It is shown that the internal energy distribution of sec-

ondary ions principally depends on the energy per atom or the velocity of the cluster ion beam ($E/n \propto v^2$). Under low energy per atom ($E/n < 10$ eV), the mean internal energy and fragmentation yield increase rapidly with the incident energy of individual constituents. Beyond 10 eV/atom impact (up to 40 eV/atom), the internal energy reaches a plateau and remains constant. Results were compared with those generated from bismuth cluster impacts for which the mean internal energies correspond well to the plateau values for argon clusters. However, a significant difference was found between argon and bismuth clusters concerning the damage or disappearance cross section. A 20 times smaller disappearance cross section was measured under 20 keV Ar_{2000}^+ impact compared to 25 keV Bi_5^+ bombardment, thus quantitatively showing the low damage effect of large argon clusters for almost the same molecular ion yield.

Keywords: TOF-SIMS, Internal energy, Bismuth cluster, Argon cluster, Benzylpyridinium ion

Introduction

Secondary ion mass spectrometry (SIMS) has been applied to analyze organic substances under static condition, i.e., with primary ion dose below 10^{13} ions/cm². This condition ensures that every impact is on an intact area to avoid sampling of damaged surfaces [1]. As a result, a very small proportion of the surface material is sputtered and of which less than 1% is

ionized [2], leading to very low secondary ion yields. Consequently, considerable efforts have been put into the development of more efficient polyatomic ion beams to increase the sputter efficiency and the secondary ion yield. Among the most widely exploited cluster ion beams, SF_6 neutral beam [3] and SF_5^+ ion beam [4] were demonstrated to greatly enhance secondary ion yield and reduce sample damage in characterizing organic polymers. The non-linear enhancement of secondary ion yields by Au_n^{q+} was reported by Blain et al. [5] and Benguerba et al. [6], and later Bi_n^{q+} by Touboul et al. [7], both of which have been intensively applied to molecular imaging ever since. In particular, much attention has been drawn to C_{60} ion beam since it became a routine ion source in TOF-SIMS [8, 9]. C_{60} bombardment illustrates greatly enhanced secondary

Electronic supplementary material The online version of this article (<https://doi.org/10.1007/s13361-018-2090-z>) contains supplementary material, which is available to authorized users.

Correspondence to: David Touboul; e-mail: david.touboul@cnsr.fr

ion yields especially for molecular ions and significantly smaller damage cross section, which result in a number of applications in depth profiling and 3D imaging [10–12]. Nevertheless, despite the secondary ion yield enhancement with the above cluster ion projectiles, the molecular damage caused by the energetic ion beams is still prominent.

The use of large argon clusters [13] to analyze organic samples was first proposed by Ninomiya et al. [14, 15] and was proved to be able to ionize amino acid and small peptide without causing significant fragmentation, implying that a soft ionization process might take place under the impact. Large argon clusters are typically composed of hundreds to thousands constituents, resulting in extremely low energy per atom E/n . Thus, it is suggested that the “soft” sputtering associated with large argon clusters is due to the low incident energy of the constitutional atoms arriving on the target. Those low-energy projectiles induce a very short range of penetration into the solid material so that the energy is deposited within the first layers of the surface without causing damage to the underneath layers. However, the ionization/desorption mechanism of the analytes involved in such bombardment is still poorly understood.

We herein propose to examine the internal energy distribution of the secondary ions (SIs), namely the internal energy imparted to desorbed ions by projectiles during the impacts. Survival yield measurements were implemented to determine internal energy distributions of SIs produced from argon and bismuth clusters bombardments, respectively. This approach has been previously applied to determine the internal energy of species produced from fast atom bombardment (FAB) [16, 17], matrix-assisted laser desorption/ionization (MALDI) [18], electrospray ionization (ESI) [19, 20], which are well-recognized methods of “soft” ionization, as well as gold nanoparticle impact at high energy [21, 22]. Thus, the “softness” of the ionization process under massive argon cluster bombardment was evaluated and compared with small bismuth clusters.

Experimental

Sample Preparation

Benzylpyridinium (BYP) salts were generously provided by Prof. D. Rondeau (Univ. de Bretagne Occidentale, Brest, France) except the *p*-cyanobenzylpyridinium salt which was purchased from Otava Chemicals Ltd. (Kyiv, Ukraine). They were separately prepared in MeOH/H₂O (1:1) and mixed before TOF-SIMS analyses. *p*-CH₃, *p*-OCH₃, *p*-NO₂, *p*-Cl, *p*-F substituted BYP ion solutions were mixed together to form one solution, while *p*-CN, *m*-CH₃, *m*-OCH₃ substituted BYP ions and 1-benzylpyridinium were mixed to obtain another. This approach permits to perform the measurements with the same projectiles under exactly the same conditions of surface, impact, and detection efficiency. Of each mixed solution, 0.5 μ L was deposited onto a gold plate and allowed to dry in air before analysis.

TOF-SIMS Analysis

MS experiments were performed with a commercial TOF-SIMS IV (ION-TOF GmbH, Münster, Germany) mass spectrometer equipped with a bismuth liquid metal ion gun (LMIG) and argon gas cluster ion beam (GCIB). In the present instrumental setup [7, 23], the Bi-LMIG is able to deliver pulsed and mass selected Bi_{*n*} (*n* = 1–7) ions with single or double charges. The Bi_{*n*}^{q+} ions were accelerated to kinetic energies of either 25 \times q keV or 12.5 \times q keV. The pulse durations of the primary ion beams were adjusted to keep a relatively low Poisson correction factor around or less than 1.1 so that saturation of the detection was negligible. Consequently, the target currents of the Bi_{*n*}^{q+} beams measured at 10 kHz were generally below 0.1 pA. All the primary ions were bunched for the sake of a typical mass resolution of 5300 at *m/z* 204. The GCIB ion column produce giant argon cluster ions of which the sizes vary from few hundreds up to 10,000. A 90° pulsing system was used to generate short pulsed ion beams with a mass resolution of 60–120. Details about the performance of this setup have been described previously [24]. In this report, different beam energies were investigated: the 20 keV energy argon clusters were selected to study the size dependence of internal energy distribution of secondary ions because of the attainable wide range of argon cluster sizes and certain 10 keV, 15 keV, and 20 keV argon clusters were selected to examine the influence of cluster size and impact energy at given velocities (E/n = 2, 5, 10, 20 eV/atom). The beam currents of argon cluster ions were typically below 0.05 pA at 10 kHz. The incident angle was 45° for both bismuth and argon cluster ion beams. Secondary ions were extracted into a single-stage reflectron-type analyzer with kinetic energies of 2 keV and then post-accelerated to 10 keV before reaching a hybrid detector composed of a single microchannel plate followed by a scintillator and a photomultiplier. The electron flood gun was switched off during all the acquisitions because the low-energy electrons could slightly overestimate the internal energy distribution.

Mass spectra of Bi_{*n*}^{q+} impacts were recorded on an area of 100 μ m \times 100 μ m divided by 128 pixels \times 128 pixels, with ion doses of 6 \times 10⁸–4 \times 10¹⁰ ions/cm². Ar_{*n*}⁺ bombardments were carried out on a larger area of 500 μ m \times 500 μ m with ion doses lower than 8 \times 10⁸ ions/cm². Measurements of disappearance cross sections were performed on 100 μ m \times 100 μ m areas with 128 \times 128 pixels for each area. The ion doses depended on the decreasing slope of secondary ion intensity versus primary ion fluence and were about 10¹³ ions/cm² for Bi clusters and more than 10¹⁴ ions/cm² for Ar clusters, respectively. The area integration of precursor and fragment peaks was processed with SurfaceLab 6.5 (ION-TOF GmbH, Münster, Germany). Survival ion yields against dissociation energy of benzylpyridinium ions and derivatives were plotted using OriginPro 2015 (OriginLab Corporation, Northampton, USA) [25].

Table 1. Benzylpyridinium Ions Used for the Measurement of Internal Energy Distribution

R ^a	m/z (M ⁺) ^b	m/z (F ⁺) ^c	Dissociation E (eV) [21]
<i>p</i> -OCH ₃	200.11	121.06	1.840
<i>p</i> -CH ₃	184.11	105.07	2.267
<i>m</i> -CH ₃	184.11	105.07	2.417
H	170.10	91.05	2.500
<i>p</i> -NO ₂	215.08	136.04	2.843

^aSubstituent group of the BYP ions^bM⁺ for molecular ion^cF⁺ for fragment ion

Results

Determination of Internal Energy Distribution

The survival yield (SY) method for determination of internal energy distribution was previously described in detail by Gabelica et al. [26]. Briefly, a series of the so-called thermometer ions with different dissociation energies are first analyzed. Then, survival yields of thermometer ions are calculated using the formula $SY = I(M^+)/[I(M^+) + I(F^+)]$, where M⁺ is the molecular ion and F⁺ the fragment ion, followed by plotting the SYs as a function of dissociation energies. Benzylpyridinium salts can be considered suitable as thermometer ions owing to their very similar structure, the well-studied dissociation pathway leading to benzyl cation, and already calculated dissociation energies related to the property of substituent groups. In the current case, two critical conditions are assumed: no parent ion remains (SY = 0) when the dissociation energy is zero, and no fragment ions are produced (SY = 1) when the dissociation energy is 4 eV. Then, the data points were fitted with a sigmoidal curve with fixed maximum SY of 1 using the following logistic function:

$$y = \frac{a}{1 + e^{-k(x-x_c)}}$$

where a was fixed at 1, x_c corresponds to the abscissa of the inflection point and k to the steepness of the curve. It must be noted that the logistic function [27] is deemed better than the

Gaussian function for fitting our experimental data. The derivative of the sigmoidal curve gives the internal energy distribution of the desorbed thermometer ions. It must be noted that the absolute values of internal energies could be obtained by taking into account kinetic shift and replacing the critical energies by appearance energies which are energies at which the rate constant for the dissociation is equal to $1/\tau$, τ being the time scale of the experiment. As we assume that the time scale of the experiment did not vary significantly for argon clusters when changing the primary ion parameters (energy and/or size of the clusters), tabulated dissociation energies for five benzylpyridinium salts were used for the determination of internal energy distribution (Table 1). The dissociation energies employed here were calculated at CCSD(T)/BSII//B3LYP/BSI level [21].

Figure 1 shows the survival yields determined from the 20 keV Ar₅₀₀⁺ bombardments, where an overestimation of the survival yield of *p*-nitrobenzylpyridinium ion is observed after fitting the data points with a sigmoidal curve. This overestimation is probably due to the occurrence of an alternative fragmentation pathway apart from the typical one which goes through the lowest activation barrier (cleavage of C-N bond in benzylpyridine). Indeed, in the corresponding mass spectrum (Fig. 1b), the ion at m/z 169.1 which can be assigned to C₁₂H₁₁N⁺ is very likely another fragment of *p*-NO₂ BYP ion [28]. However, the *p*-NO₂ BYP ion shows the highest critical energy among the series and was retained since the same experimental procedure will be applied to all the projectiles.

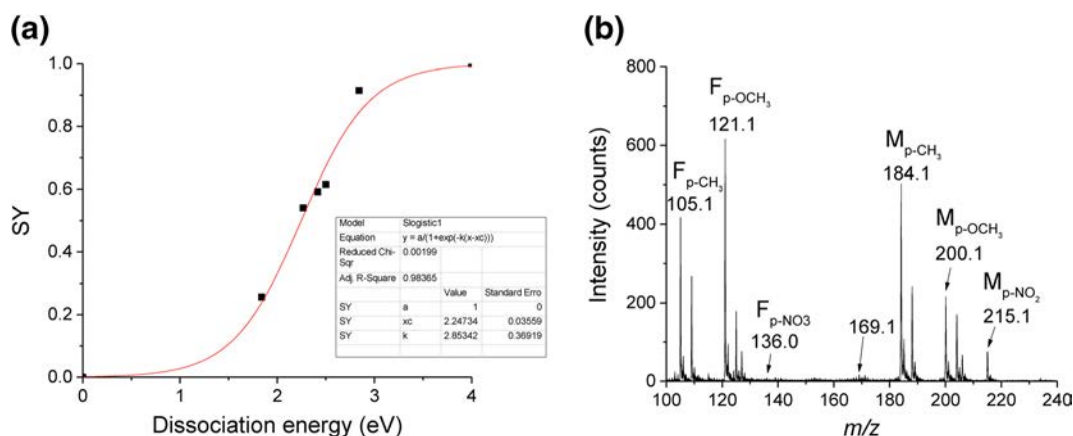


Figure 1. (a) Survival yields of five benzylpyridinium ions measured under 20 keV Ar₅₀₀⁺ bombardments, plotted as a function of dissociation energy. Red solid line is the sigmoidal fit. (b) Mass spectrum of a mixture of *p*-CH₃, *p*-OCH₃, *p*-NO₂, *p*-Cl, *p*-F substituted BYP ions acquired under the bombardment of 20 keV Ar₅₀₀⁺ ions

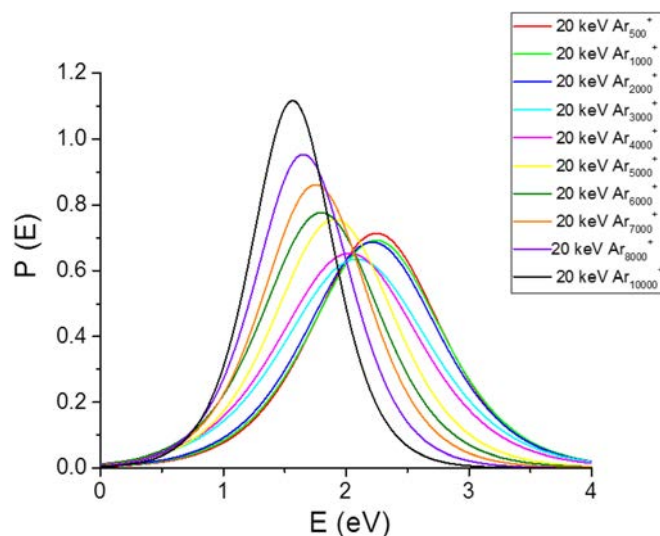


Figure 2. Internal energy distributions of SIs under impact of 20 keV argon clusters

Internal Energy Distribution of Thermometer Ions Under Argon Cluster Bombardment

Argon clusters with cluster sizes of 500–10,000 at a fixed kinetic energy of 20 keV were firstly investigated. Representative mass spectra recorded under impacts of 20 keV Ar_n^+ clusters ($n = 500, 1000, 2000, 4000, 6000, \text{ and } 8000$) are provided as supplementary data (Fig. S1). An apparent shift of internal energy distribution towards lower energy is observed as the cluster size increases at the same total energy (Fig. 2). Driven by the benefit of soft ionization in biomolecule analysis, a few experimental studies [14, 15, 29] as well

molecular dynamic simulations [30–32] have been carried out to determine the effect of cluster size on the molecular ion production. In accordance with previous reports about argon cluster bombardments on amino acid species, the present work shows that increasing the number of constituents in the argon cluster could effectively reduce fragmentation of the organic molecules to an extent that very few or no fragment ions are detected (Fig. S1) [29]. As a result, the mass spectra become much simpler and in some extent could better reveal the chemical information of the samples.

Apart from cluster size, another relevant parameter that characterizes a cluster ion beam is the energy per atom E/n which stands for the velocity of the clusters. Since the internal

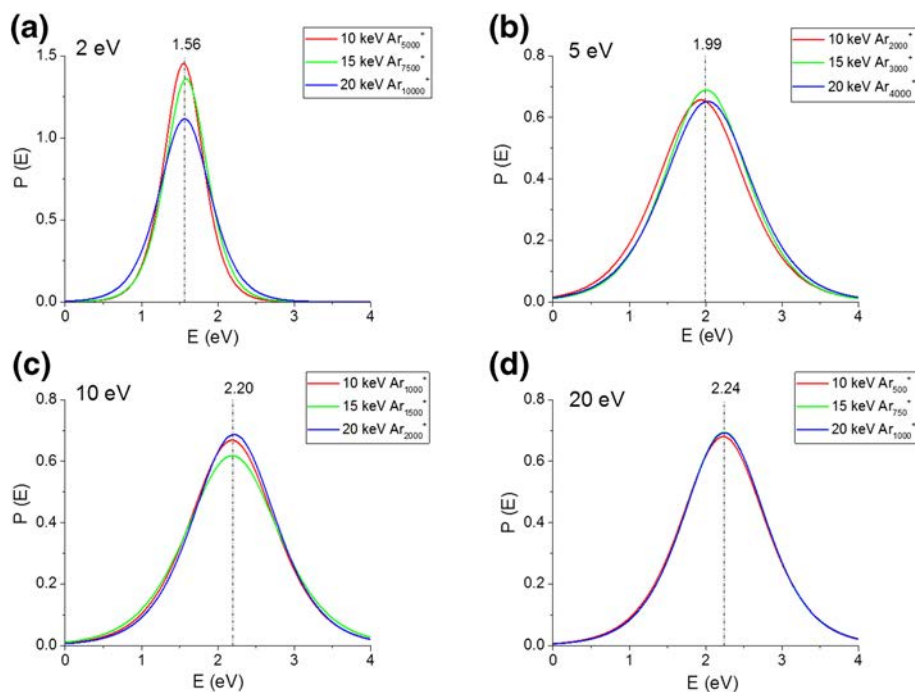


Figure 3. Internal energy distributions of secondary ions, under impact of argon clusters with different total kinetic energy and cluster sizes but same velocities (energy per atom E/n): (a) $E/n = 2$ eV; (b) $E/n = 5$ eV; (c) $E/n = 10$ eV; (d) $E/n = 20$ eV

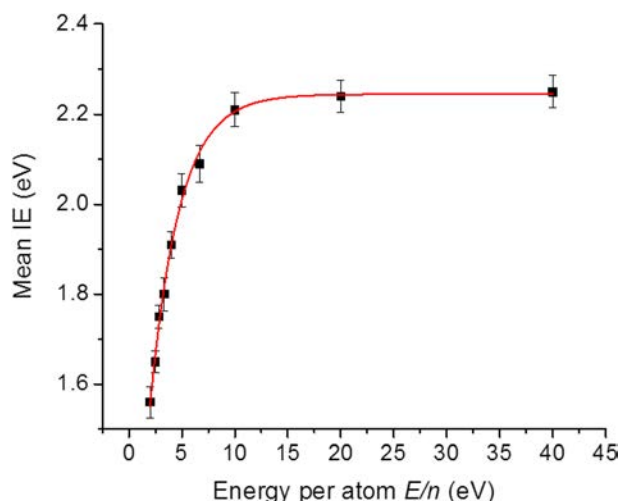


Figure 4. Mean internal energy (IE) of the secondary ions as a function of the energy per atom (E/n) of 20 keV argon clusters. The red solid line is to guide the eye

energy measured with the survival yield method depicts the internal energy imparted to the desorbed molecular ions by the projectiles during bombardment, the internal energy distribution can be affected by both impact energy of individual constituents E/n and total energy E . Figure 3 displays the internal energy distributions of secondary ions under impact of argon clusters with E/n of 2 eV, 5 eV, 10 eV, and 20 eV, respectively. Argon clusters which share the same velocity but carry different energies and constitutional numbers result in approximately the same distribution. This observation indicates

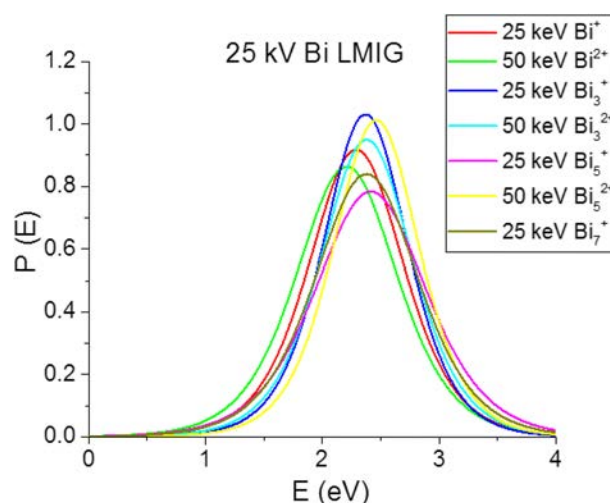


Figure 6. Internal energy distribution of thermometer ions under impacts of Bi_n^{q+} clusters with kinetic energies of 25 keV ($q=1$) and 50 keV ($q=2$)

that the internal energy distribution mainly depends on the E/n of the clusters, independent of the total kinetic energy and cluster size in this energy range. The variation in the distribution width shown in Fig. 3a is probably due to the cluster distribution of the selected ion beams. It is worth noticing that the average internal energy of the thermometer ions increases with the impact velocity, from 1.56 to 2.24 eV when the impact energy/atom raises from 2 to 20 eV/atom.

In order to establish the influence of incident velocity on the internal energy distribution of secondary ions under argon

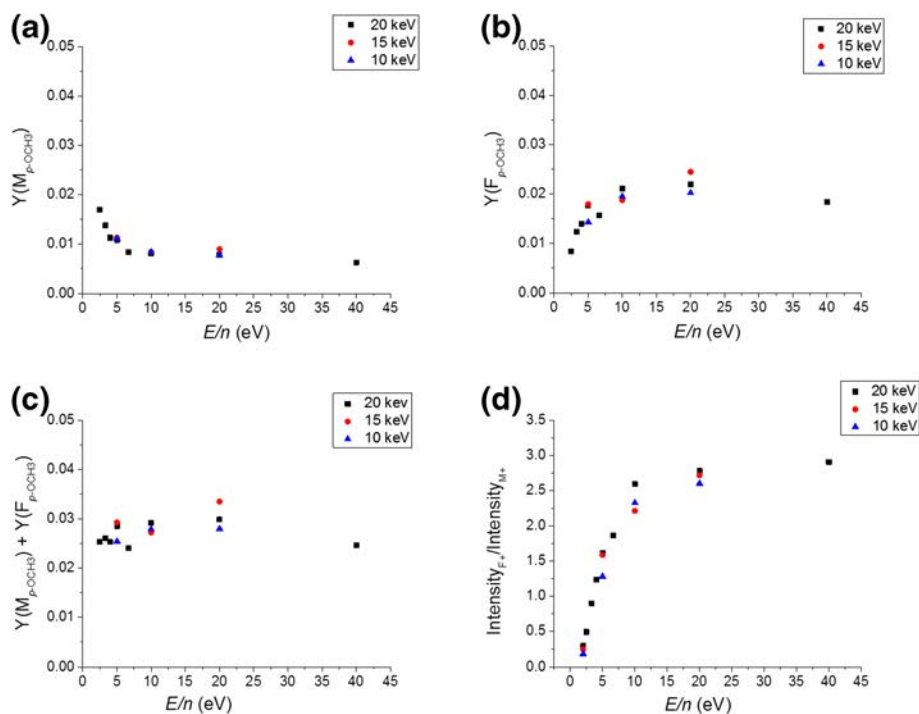


Figure 5. Influence of energy per atom E/n of argon clusters on the ion yield of (a) $p\text{-OCH}_3$ BYP molecular ion ($M_{p\text{-OCH}_3}$), (b) $p\text{-OCH}_3$ BYP fragment ion ($F_{p\text{-OCH}_3}$), (c) sum of $M_{p\text{-OCH}_3}$ and $F_{p\text{-OCH}_3}$, and (d) relative intensity of $p\text{-OCH}_3$ fragment ion ($F_{p\text{-OCH}_3}$) over molecular ion ($M_{p\text{-OCH}_3}$)

Table 2. Mean Internal Energies (IEs) Obtained for Different Bi Clusters with Accelerating Voltages of 25 kV and 12.5 kV, Respectively

Primary ion	Mean IE (eV)	
	25 kV	12.5 kV
Bi ⁺	2.29 ± 0.02	2.33 ± 0.01
Bi ²⁺	2.21 ± 0.02	2.24 ± 0.01
Bi ₃ ⁺	2.37 ± 0.01	2.37 ± 0.02
Bi ₃ ²⁺	2.38 ± 0.02	2.45 ± 0.03
Bi ₅ ⁺	2.41 ± 0.04	2.34 ± 0.03
Bi ₅ ²⁺	2.46 ± 0.03	2.39 ± 0.02
Bi ₇ ⁺	2.38 ± 0.03	2.31 ± 0.02

cluster bombardments, we then plotted the mean internal energy as a function of energy per atom E/n of the 20 keV argon clusters. As shown in Fig. 4, below $E/n = 10$ eV, the internal energy increases rapidly as the energy per atom increases. While for $E/n > 10$ eV, the mean internal energy of the SIs stays more or less constant in spite of the increasing incident energy. The raise of internal energy at low velocity impact can be easily explained by the increase in energy deposition when clusters with higher E/n hit the target. A similar increase followed by a plateau was observed experimentally by Gnaser et al. [29] when measuring the amino acid ion yield measurement as a function of the energy per atom, as well as in MD simulations where a relatively higher value of 15–20 eV was predicted for the plateau [32]. While such saturation phenomenon is not yet well understood, it may however be due to an increase of the energy dissipation under higher energy impact, as in the case of C₆₀ projectiles [33]. Therefore, only the projectile energy deposited in a certain volume could contribute to this energy transfer. Thus, it can be concluded that for organic sputtering by large argon clusters, “softer” ionization could be obtained by decreasing the energy/atom lower than 10 eV.

Examination of the secondary ion yield under the low E/n impact is illustrated for *p*-OCH₃ BYP ion in Fig. 5. The lowest energy per atom investigated here is 2.5 eV which is still able to afford an effective sputtering process providing an ion yield of 1.18×10^{-2} for the molecular ion (Fig. 5a). This may partly benefit from the readily charged target molecular ions, while it is more likely due to the enhancement effect of cluster ions. The low energy but extremely dense impacts cause more efficient sputtering than individual atoms. It is noted that effective sputtering was also observed under impact of clusters

with $E/n = 2.0$ eV (20 keV Ar₁₀₀₀₀⁺). However, the cluster ion current was too low to afford an accurate value of SY.

Figure 5 also demonstrates that the molecular ion yield of *p*-OCH₃ BYP ion decreases rapidly as E/n increases from 2.5 to 10 eV while the fragment ion yield exhibits an opposite trend, indicating an increase of fragmentation extent as the impact velocity increases. Nevertheless, the decrease of molecular ion yield may also be partly due to the metastable decay occurred during the flight to the detector [34]. In the case of *p*-OCH₃ BYP ion which has very low dissociation energy, the sum of molecular and fragment ion yields is revealed to be mostly constant irrespective of the E/n of the impacting clusters (Fig. 5c), whereas for the thermometer ions with higher dissociation energies, the fragment ion yields are so low that the plots of summed ion yields versus E/n are governed basically by the behavior of molecular ions. The dependence of fragment ion intensity/molecular ion intensity ratio with the energy per atom is in line with the plot depicting the mean internal energy as a function of E/n of the argon clusters. It is worth noticing that all the 10 keV, 15 keV, and 20 keV argon clusters with the same energy per atom gave very similar ion yield values, demonstrating the beam velocity dependence of the secondary ion yields.

It has also been shown that the secondary ion yield decrease distinctively within a certain E/n . In particular, Gnaser et al. [29] have demonstrated that the molecular intensities of amino acids are relatively constant beyond $E/n = 10$ eV while drop dramatically in the low-energy regime ($E/n < 10$ eV). This phenomenon was tentatively explained by the decrease in the number of free protons produced during the bombardment, thus reducing the protonation of sputtered molecules. In other words, the molecular ion production is mainly determined by

Table 3. Yields Y , Disappearance Cross Section σ , Secondary Ion Efficiency E Generated for *p*-Methylbenzylpyridinium Ion (m/z 184.11) and Mean Internal Energy (IE) Under Bismuth and Argon Cluster Bombardments

Voltage	PI	Current (pA at 100 μ s)	Y	σ (cm ²)	E (cm ⁻²)	Mean IE (eV)
25 kV	Bi ⁺	0.330	5.49×10^{-4}	3.87×10^{-14}	1.42×10^{10}	2.29 ± 0.02
	Bi ²⁺	0.184	4.52×10^{-3}	3.03×10^{-14}	1.49×10^{11}	2.21 ± 0.02
	Bi ₃ ⁺	0.022	4.40×10^{-2}	1.62×10^{-13}	2.72×10^{11}	2.37 ± 0.01
	Bi ₃ ²⁺	0.012	6.02×10^{-2}	2.58×10^{-13}	2.34×10^{11}	2.38 ± 0.02
	Bi ₅ ⁺	0.028	2.55×10^{-2}	9.17×10^{-14}	2.78×10^{11}	2.41 ± 0.04
	Bi ₅ ²⁺	0.026	4.18×10^{-2}	7.38×10^{-14}	5.66×10^{11}	2.46 ± 0.03
	Bi ₇ ⁺	0.006	4.48×10^{-2}	1.11×10^{-13}	4.04×10^{11}	2.38 ± 0.03
20 kV	Ar ₂₀₀₀ ⁺	0.05	1.54×10^{-2}	4.44×10^{-15}	3.47×10^{12}	2.21 ± 0.04

the ionization efficiency under low-energy impact. This assumption is confirmed by our observation that the ion yield of thermometer ions decreases with E/n of the impinging projectiles. Since there is almost no ionization barrier for the thermometer ions (BYP cations), the fragmentation will take place as soon as the received internal energy exceeds the dissociation energy, leading to the decrease of molecular ion yield.

Internal Energy Distribution of Secondary Ions Under Bismuth Cluster Bombardment

With the same instrumental configuration, the internal energy distributions of SIs under small bismuth cluster impacts were also examined for comparison. Figure 6 displays the internal energy distributions of thermometer ions under 25 keV or 50 keV Bi_n^{q+} cluster bombardments. It is revealed that the internal energy distributions obtained from different bismuth clusters are more or less similar in terms of both the mean internal energy and the width of the distribution. Further examination of Bi_n^{q+} ion beam accelerated by 12.5 kV voltage gave nearly identical results with a mean internal energy of 2.2–2.4 eV (Table 2). Rather surprising at first thought that the internal energy imparted from Bi clusters to the SIs is independent of the beam energy, however, this finding is consistent with the results from high energy per atom ($E/n > 10$ eV) argon cluster impacts, where the mean internal energy remains constant at ~ 2.24 eV. Since the energy per atom of the examined Bi clusters is far beyond 10 eV, all the data points shall fall onto the plateau and provide similar mean internal energy.

Secondary Ion Yield, Disappearance Cross Section, and Ion Efficiency Under Bismuth and Argon Cluster Bombardments

To further understand the low-energy impact of massive argon clusters, several values such as secondary ion emission yields Y , disappearance cross section σ , and secondary ion efficiency E (defined as Y/σ) obtained under argon cluster bombardment were compared with those from small bismuth cluster bombardments. The definitions and determination of these values have been comprehensively described elsewhere [23, 35]. Table 3 summarizes the cluster species and the corresponding Y , σ , and E generated for $p\text{-OCH}_3$ BYP ion, and mean internal energy (IE) values. It should be noted that only one argon cluster species is investigated here, due to the significantly small damage cross section which requires extremely long acquisition time to observe the decrease of ion intensity (the experimental data for argon cluster are depicted in Fig. S2). Upon comparison, it is revealed that the secondary ion yields obtained under 20 keV Ar_{2000}^+ cluster impact are of the same order of magnitude as those measured from bismuth cluster impacts. Meanwhile, although there is a dramatic difference in energy per atom between bismuth cluster (keV regime) and argon cluster (eV regime), the amount of energy transferred to the analytes during the bombardments proves to be very similar. However, it is worth noticing that the disappearance cross

section for large argon cluster bombardment ($4.44 \times 10^{-15} \text{ cm}^2$) is over 20 times smaller than that for 25 keV Bi_5^+ cluster bombardment ($9.17 \times 10^{-14} \text{ cm}^2$), resulting in a much higher secondary ion efficiency of $3.47 \times 10^{12} \text{ cm}^{-2}$. These values directly show that large argon cluster sputtering induces greatly reduced sample damage, consistent with previous comparison studies with C_{60}^+ projectile [36, 37].

Conclusion

Examination of internal energy distributions of the thermometer ions allowed us to evaluate the “softness” of the ionization process of cluster bombardments. Results show that larger argon clusters, especially those with $E/n < 5$ eV, give lower and narrower internal energy distributions, implying a “softer” ionization process. Moreover, the fragmentation yield increases with the incident energy of individual constituents when E/n is less than 10 eV, whereas a saturation state arises with E/n exceeding 10 eV.

Under keV bismuth cluster impacts, all the Bi_n^{q+} species gave similar internal energy distributions with mean internal energy values close to those obtained under $E/n > 10$ eV argon cluster impact. Therefore, the relatively constant mean internal energy values obtained from bismuth cluster impact might correspond to the plateau shown in Fig. 5, and this plot may possibly present the universal behavior of the cluster impact in TOF-SIMS. However, further investigation of a wider range of projectiles will be required to verify this hypothesis.

In addition, compared with bismuth clusters, argon cluster impact provides similar secondary ion yield but much higher secondary ion efficiency owing to the significantly smaller disappearance cross section.

Acknowledgements

This work was supported by the Agence Nationale de la Recherche (grant ANR-2015-CE29-0007-01 DEFIMAGE). TF would like to acknowledge financial support from China Scholarship Council (CSC, No. 201406310013) for her PhD studies [25].

References

1. Benninghoven, A., Jaspers, D., Sichtermann, W.: Secondary-ion emission of amino acids. *Appl. Phys.* **11**, 35–39 (1976)
2. Benninghoven, A., Hagenhoff, B., Niehuis, E.: Surface MS: probing real-world samples. *Anal. Chem.* **65**, 630A–640A (1993)
3. Appelhans, A.D., Delmore, J.E., Dahl, D.A.: Focused, rasterable, high-energy neutral molecular beam probe for secondary ion mass spectrometry. *Anal. Chem.* **59**, 1685–1691 (1987)
4. Gillen, G., Roberson, S.: Preliminary evaluation of an SF_5 polyatomic primary ion beam for analysis of organic thin films by secondary ion mass spectrometry. *Rapid Comm. Mass Spectrom.* **12**, 1303–1312 (1998)
5. Blain, M.G., Della-Negra, S., Joret, H., Le Beyec, Y., Schweikert, E.A.: Secondary-ion yields from surfaces bombarded with keV molecular and cluster ions. *Phys. Rev. Lett.* **63**, 1625–1628 (1989)
6. Benguerba, M., Brunelle, A., Della-Negra, S., Depauw, J., Joret, H., Le Beyec, Y., Blain, M.G., Schweikert, E.A., Ben Assayag, G., Sudraud, P.:

- Impact of slow gold cluster on various solids: nonlinear effects in secondary ion emission. *Nucl. Instrum. Methods Phys. Res. B.* **62**, 8–22 (1991)
7. Touboul, D., Kollmer, F., Niehuis, E., Brunelle, A., Lapr vate, O.: Improvement of biological time-of-flight-secondary ion mass spectrometry imaging with a bismuth cluster ion source. *J. Am. Soc. Mass Spectrom.* **16**, 1608–1618 (2005)
 8. Boussofi ne-Baudin, K., Bolbach, G., Brunelle, A., Della-Negra, S., H kansson, P., Le Beyec, Y.: Secondary ion emission under cluster impact at low energies (5–60 keV); influence of the number of atoms in the projectile. *Nucl. Instrum. Methods Phys. Res. B.* **88**, 160–163 (1994)
 9. Weibel, D., Wong, S., Lockyer, N., Blenkinsopp, P., Hill, R., Vickerman, J.C.: A C₆₀ primary ion beam system for time of flight secondary ion mass spectrometry: its development and secondary ion yield characteristics. *Anal. Chem.* **75**, 1754–1764 (2003)
 10. Fletcher, J.S., Lockyer, N.P., Vickerman, J.C.: Developments in molecular SIMS depth profiling and 3D imaging of biological systems using polyatomic primary ions. *Mass Spectrom. Rev.* **30**, 142–174 (2011)
 11. Robinson, M.A., Graham, D.J., Castner, D.G.: ToF-SIMS depth profiling of cells: z-correction, 3D imaging, and sputter rate of individual NIH/3T3 fibroblasts. *Anal. Chem.* **84**, 4880–4885 (2012)
 12. Tian, H., Six, D.A., Krucker, T., Leeds, J.A., Winograd, N.: Subcellular chemical imaging of antibiotics in single bacteria using C₆₀-secondary ion mass spectrometry. *Anal. Chem.* **89**, 5050–5057 (2017)
 13. Yamada, I., Matsuo, J., Toyoda, N., Kirkpatrick, A.: Materials processing by gas cluster ion beams. *Mater. Sci. Eng. R.* **34**, 231–295 (2001)
 14. Ninomiya, S., Nakata, Y., Ichiki, K., Seki, T., Aoki, T., Matsuo, J.: Measurements of secondary ions emitted from organic compounds bombarded with large gas cluster ions. *Nucl. Instrum. Methods Phys. Res. B.* **256**, 493–496 (2007)
 15. Ninomiya, S., Nakata, Y., Honda, Y., Ichiki, K., Seki, T., Aoki, T., Matsuo, J.: A fragment-free ionization technique for organic mass spectrometry with large Ar cluster ions. *Appl. Surf. Sci.* **255**, 1588–1590 (2008)
 16. De Pauw, E., Pelzer, G., Marien, J., Natalis, P.: Internal energy distribution of ions emitted in secondary ion mass spectrometry. *Springer Proc. Phys.* **9**, 103–108 (1986)
 17. Derwa, F., De Pauw, E., Natalis, P.: New basis for a method for the estimation of secondary ion internal energy distribution in ‘soft’ ionization techniques. *Org. Mass Spectrom.* **26**, 117–118 (1991)
 18. Luo, G., Marginean, I., Vertes, A.: Internal energy of ions generated by matrix-assisted laser desorption/ionization. *Anal. Chem.* **74**, 6185–6190 (2002)
 19. Collette, C., De Pauw, E.: Calibration of the internal energy distribution of ions produced by electrospray. *Rapid Comm. Mass Spectrom.* **12**, 165–170 (1998)
 20. Touboul, D., Jecklin, M.C., Zenobi, R.: Ion internal energy distributions validate the charge residue model for small molecule ion formation by spray methods. *Rapid Comm. Mass. Spectrom.* **22**, 1062–1068 (2008)
 21. DeBord, J.D., Verkhoturov, S.V., Perez, L.M., North, S.W., Hall, M.B., Schweikert, E.A.: Measuring the internal energies of species emitted from hypervelocity nanoparticle impacts on surfaces using recalibrated benzylpyridinium probe ions. *J. Chem. Phys.* **138**, 214301 (2013)
 22. DeBord, J.D., Fernandez-Lima, F.A., Verkhoturov, S.V., Schweikert, E.A., Della-Negra, S.: Characteristics of positive and negative secondary ions emitted from Au₃⁺ and Au₄₀₀⁺⁴ impacts. *Surf. Interface Anal.* **45**, 134–137 (2013)
 23. Brunelle, A., Touboul, D., Lapr vate, O.: Biological tissue imaging with time-of-flight secondary ion mass spectrometry and cluster ion sources. *J. Mass Spectrom.* **40**, 985–999 (2005)
 24. Kayser, S., Rading, D., Moellers, R., Kollmer, F., Niehuis, E.: Surface spectrometry using large argon clusters. *Surf. Interface Anal.* **45**, 131–133 (2013)
 25. Fu T. 3D and high sensitivity micrometric mass spectrometry imaging. Ph.D. Thesis, Analytical Chemistry, Universit  Paris-Saclay, 2017; <https://tel.archives-ouvertes.fr/tel-01699065v2/document>. Accessed May 24, 2018.
 26. Gabelica, V., De Pauw, E.: Internal energy and fragmentation of ions produced in electrospray sources. *Mass Spectrom. Rev.* **24**, 566–587 (2005)
 27. Reed, L.J., Berkson, J.: The application of the logistic function to experimental data. *J. Phys. Chem.* **33**, 760–779 (1929)
 28. Barylyuk, K.V., Chingin, K., Balabin, R.M., Zenobi, R.: Fragmentation of benzylpyridinium “thermometer” ions and its effect on the accuracy of internal energy calibration. *J. Am. Soc. Mass Spectrom.* **21**, 172–177 (2010)
 29. Gnaser, H., Ichiki, K., Matsuo, J.: Strongly reduced fragmentation and soft emission processes in sputtered ion formation from amino acid films under large Ar_n⁺ (n ≤ 2200) cluster ion bombardment. *Rapid Commun. Mass Spectrom.* **26**, 1–8 (2012)
 30. Rzeznik, L., Czerwinski, B., Garrison, B.J., Winograd, N., Postawa, Z.: Molecular dynamics simulations of sputtering of organic overlayers by slow, large clusters. *Appl. Surf. Sci.* **255**, 841–843 (2008)
 31. Rzeznik, L., Czerwinski, B., Garrison, B.J., Winograd, N., Postawa, Z.: Microscopic insight into the sputtering of thin polystyrene films on Ag{111} induced by large and slow Ar clusters. *J. Phys. Chem. C.* **112**, 521–531 (2008)
 32. Delcorte, A., Garrison, B.J., Hamraoui, K.: Dynamics of molecular impacts on soft materials: from fullerenes to organic nanodrops. *Anal. Chem.* **81**, 6676–6686 (2009)
 33. Russo, M.F., Garrison, B.J.: Mesoscale energy deposition footprint model for kiloelectronvolt cluster bombardment of solids. *Anal. Chem.* **78**, 7206–7210 (2006)
 34. Luxembourg, S.L., Heeren, R.M.A.: Fragmentation at and above surfaces in SIMS: effects of biomolecular yield enhancing surface modifications. *Int. J. Mass Spectrom.* **253**, 181–192 (2006)
 35. K tter, F., Benninghoven, A.: Secondary ion emission from polymer surfaces under Ar⁺, Xe⁺ and SF₅⁺ ion bombardment. *Appl. Surf. Sci.* **133**, 47–57 (1998)
 36. Rabbani, S., Barber, A.M., Fletcher, J.S., Lockyer, N.P., Vickerman, J.C.: TOF-SIMS with argon gas cluster ion beams: a comparison with C₆₀⁺. *Anal. Chem.* **83**, 3793–3800 (2011)
 37. Shard, A.G., Havelund, R., Seah, M.P., Spencer, S.J., Gilmore, I.S., Winograd, N., Mao, D., Miyayama, T., Niehuis, E., Rading, D., Moellers, R.: Argon cluster ion beams for organic depth profiling: results from a VAMAS interlaboratory study. *Anal. Chem.* **84**, 7865–7873 (2012)